Bright narrowband biphoton generation from a hot rubidium atomic vapor cell

Lingbang Zhu, Xianxin Guo, Chi Shu, Heejeong Jeong, and Shengwang Du

CrossMark
←click for updates

Bright narrowband biphoton generation from a hot rubidium atomic vapor cell

Lingbang Zhu,[1,a)] Xianxin Guo,[1,a)] Chi Shu,[2] Heejeong Jeong,[1,3,b)] and Shengwang Du[1,b)]

[1]*Department of Physics, The Hong Kong University of Science and Technology, Clear Water Bay, Kowloon, Hong Kong, China*
[2]*Department of Physics, Harvard University, Cambridge, Massachusetts 02138, USA*
[3]*Institute for Advanced Study, The Hong Kong University of Science and Technology, Clear Water Bay, Kowloon, Hong Kong, China*

We demonstrate the generation of high-quality narrowband biphotons from a Doppler-broadened hot rubidium atomic vapor cell. Choosing a double-Λ atomic energy level scheme for optimizing both spontaneous four-wave mixing nonlinear parametric interaction and electromagnetically induced transparency (EIT), we achieve a biphoton spectral brightness as high as $14\,000\,\mathrm{s}^{-1}\,\mathrm{MHz}^{-1}$. Meanwhile, we apply a spatially tailored optical pumping beam for reduction of the Raman noise and obtain a violation of the Cauchy-Schwarz inequality by a factor of 1023. *Published by AIP Publishing.*
[http://dx.doi.org/10.1063/1.4980073]

Quantum-network protocols based on efficient atom-photon interactions require entangled photons with a bandwidth narrower than the atomic natural linewidth (about 10 MHz).[1] Using the conventional method of spontaneous parametric down conversion with nonlinear crystals, biphoton generation with such a bandwidth requires implementing a single-mode cavity with special care.[2–4] In free space, spontaneous four-wave mixing (SFWM) in laser-cooled atoms has been demonstrated as an effective method in producing subnatural-linewidth biphotons,[5–7] but cold atom apparatuses are large, expensive, and require a complicated operation.

Recently, we demonstrated the generation of subnatural-linewidth (2 MHz) biphotons from a Doppler-broadened hot [87]Rb vapor cell,[8] which provides a possibility of miniaturized narrowband biphoton source based on free-space atomic vapor cell. The paraffin coating in increasing the ground-state coherence time and the spatially separated optical pumping were the two keys in suppressing on-resonance Raman scattering noise photons. However, the scheme demonstrated in Ref. 8 can still be further optimized. First, the double-Λ atomic energy levels can be carefully chosen to maximize the third-order nonlinearity for enhancing the photon pair generation efficiency and the brightness. Second, the spatial profile of the optical pumping beam can be optimized to improve the optical pumping efficiency and minimize the Raman scattering noise.

In this letter, we demonstrate an optimized scheme for hot [87]Rb atomic-vapor-cell-based narrowband biphoton source. Compared to our previous work in Ref. 8, we carefully choose new energy levels with a higher third-order nonlinear susceptibility to increase the photon pair generation rate by a factor of 2.5. Meanwhile, we design a spatially hollow beam for the optical pumping laser to effectively shield the atoms in the SFWM volume for reducing the uncorrelated noise photons from the on-resonance Raman scattering.

By operating the system at a temperature of 66 °C with the upgraded optical pumping, we achieve a biphoton rate as high as $40\,000\,\mathrm{s}^{-1}$.

Figure 1 illustrates schematics of our experimental setup. Driven by two vertically (V) polarized counter-propagating pump laser (780 nm, ω_p) and coupling laser (795 nm, ω_c) beams, phase-matched and backward Stokes (ω_s) and anti-Stokes (ω_{as}) photon pairs are spontaneously generated from a paraffin-coated hot [87]Rb vapor cell. The generated photon pairs are sent to two polarization beam splitters (PBS) as polarization filters and coupled into two opposing single mode fibers (SMF). After going through two optical frequency filters (F_s and F_{as}), the photon pairs are detected by two single-photon counting modules (SPCM$_s$ and SPCM$_{as}$, Excelitas SPCM-AQRH-16-FC). We use a time-to-digit converter (Fast Comtec P7888) with 1 ns bin width to record the coincidence counts. The fiber coupling efficiency and SPCM detection efficiency are 70% and 50%, respectively. We also consider the polarizer efficiency, which is 80%. The etalon filters have free spectrum range FSR = 13.6 GHz. The bandwidth, transmission efficiency, and extinction ratio of the frequency filters are 350 MHz, 60%, and 60 dB for F_s; and 80 MHz, 40%, and 40 dB for F_{as}. To spatially separate the generated biphotons, the pump and coupling laser beams are aligned with an angle of 0.2° to the biphoton collection directions.

Figure 2 shows the effect of the SFWM energy-level scheme on the biphoton generation rate. The pump laser is red detuned by 2.7 GHz from the transition $|5S_{1/2}, F = 1\rangle \rightarrow |5P_{3/2}, F = 2\rangle$. To depopulate the upper ground state, $|5S_{1/2}, F = 2\rangle$, we apply a strong hollow-shaped optical pumping beam at the frequency of ω_{op}, which is tuned to the transition $|5S_{1/2}, F = 2\rangle \rightarrow |5P_{3/2}, F = 1\rangle$. In the first case, the same as the previous experiment,[8] as shown in the inset of Fig. 2(a), we set the coupling laser to the on-resonance transition $|5S_{1/2}, F = 2\rangle \rightarrow |5P_{1/2}, F = 1\rangle$ and the anti-Stokes photons are generated from the transition $|5P_{1/2}, F = 1\rangle \rightarrow |5S_{1/2}, F = 1\rangle$. In our optimal energy scheme as shown in the inset of
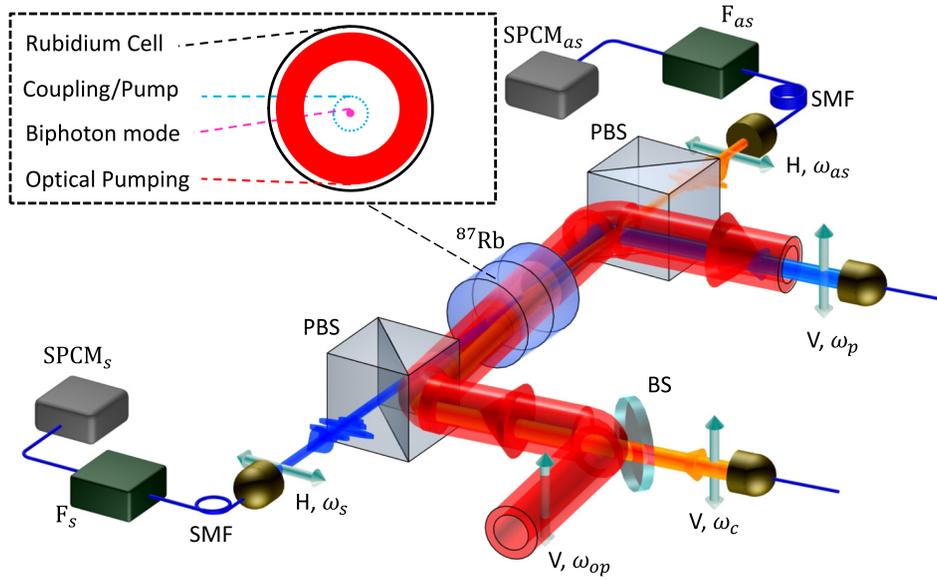
FIG. 1. Experimental scheme to generate narrowband biphotons from a hot ^{87}Rb vapor cell. In the presence of counter-propagating vertically (V) polarized pump (780 nm, ω_p) and coupling (795 nm, ω_c) laser beams, horizontally (H) polarized counter-propagating phase-matched Stokes (ω_s) and anti-Stokes (ω_{as}) photon pairs are spontaneously generated. In the inset, we make a zoom-in on the transverse cross section of a cell to clearly show the beam profiles of all incident lasers and the biphoton. The biphoton mode has a waist diameter $(1/e^2)$ of 250 μm focused in the middle of the 1.27-cm-long cell. The collimated coupling and pump laser beams have the same $1/e^2$ beam diameter of 1.4 mm. The hollow optical pumping beam has an outer diameter of 10 mm and inner diameter of 4 mm. Thus, the hollow beam does not overlap with the SFWM volume enclosed by the pump and coupling beams. The inner diameter of the cell is 10 mm.

Fig. 2(b), we tune the coupling laser to the transition $|5S_{1/2}, F=2\rangle \rightarrow |5P_{1/2}, F=2\rangle$, and thus, the anti-Stokes photons are generated in the transition $|5P_{1/2}, F=2\rangle \rightarrow |5S_{1/2}, F=1\rangle$. We note that the on-resonance two-level absorption cross section changes from $\lambda_{as}^2/(12\pi)$ in the previous energy-level scheme to $5\lambda_{as}^2/(12\pi)$ in the optimal scheme. That is, the electric dipole matrix element of the anti-Stokes transition in the optimal scheme increases by a factor of $\sqrt{5}$ as compared to the previous energy-level scheme.[11] The electric dipole matrix element of the coupling transition remains the same in both schemes. Consequently, the SFWM third-order nonlinear susceptibility increases by a factor of $\sqrt{5}$. As confirmed by the measurement of coincidence counts in Figs. 2(a) and 2(b), the photon pair counts increase by a factor of about 3. The solid curves in Figs. 2(a) and 2(b) are obtained following the theoretical treatment in Refs. 8 and 10, showing the perfect agreement with the experimental data.

Next, we engineer the spatial profile of the optical pumping beam to suppress the noise from on-resonance Raman scattering of the coupling laser beam because of residual atoms in the upper ground state, $|5S_{1/2}, F=2\rangle$. In the previous experiment, the cross-sectional beam profile was Gaussian shape,[8] which was located aside from the SFWM volume. To increase the interaction area of optical pumping, we use a hollow-shaped beam in this work, as shown in the inset of Fig. 1. Compared to the previously used Gaussian beam, the hollow beam depopulates the upper ground state more efficiently, since we optically pump all the atoms colliding on the paraffin-coated wall and then moving toward SFWM region. Figure 3 shows a comparison of the hollow-beam optical pumping method to the Gaussian beam. In order not to interfere with the EIT-assisted SFWM process, we block the center of the enlarged Gaussian beam (1 cm diameter) with a 4 mm dark spot and make the light intensity zero at

the center. Thus, the hollow-shaped optical pumping beam covers most of the area for depopulating the upper ground state ($|5S_{1/2}, F=2\rangle$) and suppresses uncorrelated photons from the on-resonance Raman scattering of the coupling laser arising from the same central frequency and polarization as the anti-Stokes photons following the transition: $|5S_{1/2}, F=2\rangle \rightarrow |5P_{1/2}, F=1\rangle \rightarrow |5S_{1/2}, F=1\rangle$. The results indicate a significant improvement in the biphoton signal contrast ratio ($[g_{s,as}^{(2)}]_m$, the peak value of the normalized cross correlation function $[g_{s,as}^{(2)}](\tau)$) for the case of the hollow optical pumping beam. The value increases rapidly at low optical pumping power until it reaches 10 mW and slowly increases up to the optimum value at 60 mW, then saturates for higher powers.

With the above two optimizations, we now characterize the biphoton source. For biphotons generated from SFWM process, the photon pair rate depends on the pump power and optical depth. Thus, we scan the pump power by setting the vapor cell at two temperatures 59 °C and 66 °C. Figure 4 shows that the biphoton rate increases linearly with pump power, while $[g_{s,as}^{(2)}]_m$ decreases monotonically both in log-log scale. Specifically, at T = 66 °C and the maximum pump power of 60 mW, we obtain a biphoton rate of about $40\,000\,\text{s}^{-1}$ with correction of signal collection efficiency. With the biphoton bandwidth of 2.9 MHz, the spectral brightness is about $14\,000\,\text{s}^{-1}\,\text{MHz}^{-1}$ with a signal contrast ratio of about 6. At T = 59 °C and the minimum pump power of 0.75 mW, the rate and the signal contrast ratio are $345\,\text{s}^{-1}$ and 56, respectively. The high biphoton signal contrast ratio in our system indicates a strong violation of the Cauchy-Schwarz inequality $[g_{s,as}^{(2)}(\tau)]^2/[g_{s,s}^{(2)}(0)g_{as,as}^{(2)}(0)] \leq 1$.[9] With the measured autocorrelations $g_{s,s}^{(2)}(0) = 1.88 \pm 0.15$ and $g_{as,as}^{(2)}(0) = 1.63 \pm 0.13$, the signal contrast ratio of 56 (6) corresponds to violation of the Cauchy-Schwarz inequality by a factor of
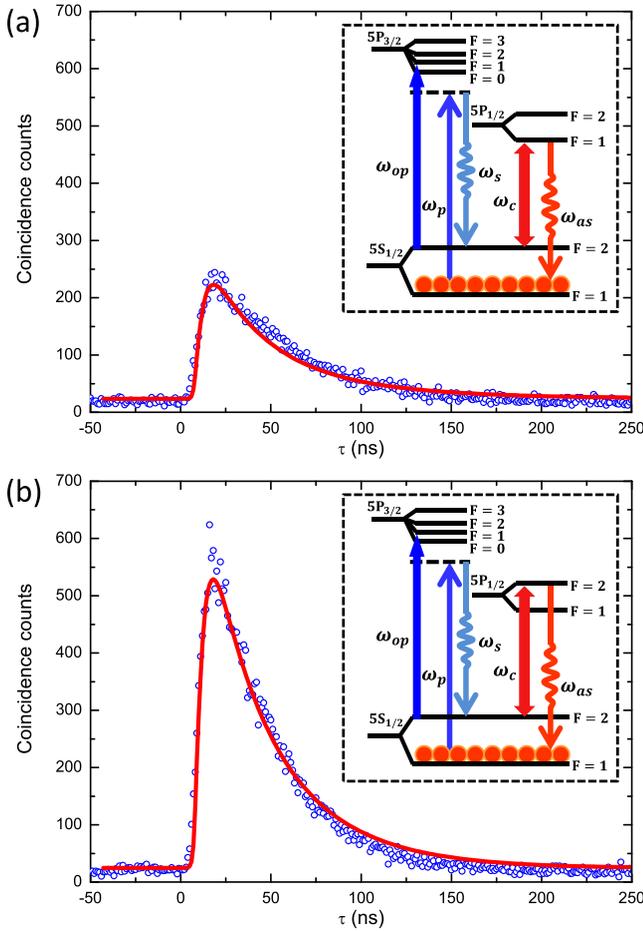
FIG. 2. Biphoton waveforms with two different SFWM energy-level schemes: (a) the scheme used in the previous work,[8] and (b) the optimal scheme in this work. The two-photon coincidence counts are collected over 300 s with 1 ns bin width, as a function of the relative time delay τ between the paired Stokes and anti-Stokes photons. The insets denote the relevant [87]Rb atomic energy-level diagram. The incident pump and coupling laser powers are 6 mW and 10 mW, respectively. The hollow-shape optical pumping power is 80 mW, and the temperature of the cell is 59 °C. The blue circles denote the experimental data while the solid red theoretical curves.

FIG. 3. Optical pumping effect with hollow and Gaussian beam profiles for the optimal energy-level scheme. The measured $[g^{(2)}_{s,as}]_m$ is plotted as a function of optical pumping laser power. The pump laser power and coupling laser power are fixed at 6 mW and 10 mW, respectively. The cell temperature is 59 °C.

1023 (12). The flexibility of our system in obtaining a high biphoton rate or a high $[g^{(2)}_{s,as}]_m$ value makes it a versatile quantum platform. Note that overall values are higher than the previous results of Ref. 8. The maximum value of the contrast ratio $[g^{(2)}_{s,as}]_m$, 56, is about five times higher than 12, the value that appeared in the previous research.[8] Besides, the overall photon pair rate ($\sim$40 000 s^{-1}) is also about more than 20 times higher than that obtained in Ref. 8.

The biphoton coherence time, and thus the bandwidth, can be tuned with EIT by varying the coupling laser power. Fig. 5(a) shows biphoton waveforms as functions of relative time delay τ at coupling laser powers of 20 and 3 mW, respectively. As expected, the $1/e$ correlation time increases from 40 to 85 ns as we reduce the coupling laser power. The insets of Figs. 5(a1) and 5(a2) are the measured conditional auto-correlation $g^{(2)}_c$ as functions of time-bin width.[12] Within the correlation time, the values of $g^{(2)}_c$ are far below two-photon threshold, 0.5. Figure 5(b) shows the $1/e$ correlation times (red squares) and $[g^{(2)}_{s,as}]_m$ (blue circle) as functions of the coupling power. This inversely proportional relationship of decay time with coupling power can easily be explained
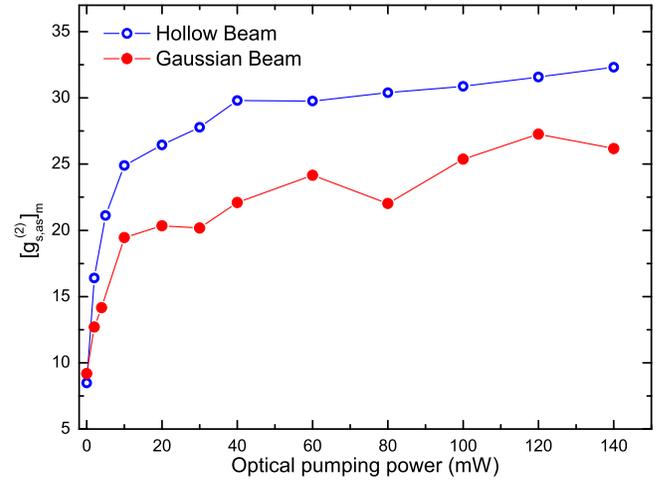
by the slow light group delay associated with the EIT spectrum. The bandwidths of these biphotons in Figs. 5(a1) and 5(a2) are 4.0 MHz and 1.9 MHz, respectively. They are comparable or substantially narrower than the natural linewidth of 6 MHz of Rb atoms. Figure 5(b) also shows that we obtain the optimum value of $[g^{(2)}_{s,as}]_m$ at 10 mW coupling power.

To conclude, we have optimized the generation of narrowband ($\sim$2 MHz) biphotons from a hot Rb atomic vapor cell with a high contrast ratio of 56, and a bright photon pair rate of 40 000 s^{-1}. The biphoton spectral brightness reaches as high as 14 000 s^{-1} MHz^{-1} in our hot atomic vapor cell system. This bright signal is due to two key improvements: one is to increase the biphoton generation rate by more than two times with a new energy-level configuration and the other is to further reduce the noise by a half, utilizing the spatially tailored hollow beam for optical pumping. Our hot-atomic biphoton generator might be useful in quantum information applications, such as a quantum repeater[13] or in quantum key distribution.[14,15]
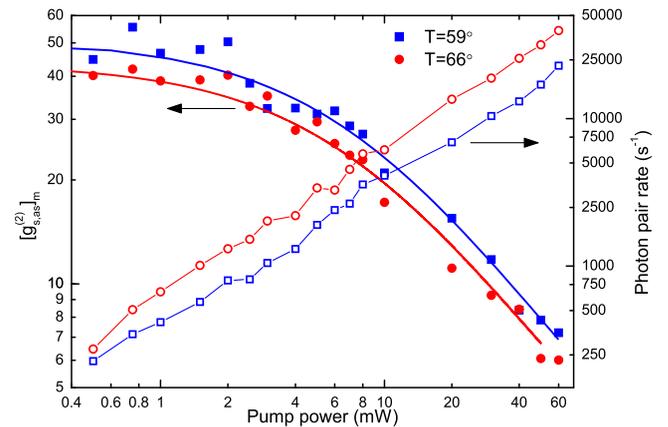

FIG. 4. Biphoton generation at different pump laser power under two cell temperatures. The pump and coupling laser powers are fixed at 6 mW and 10 mW, respectively. The hollow-shaped optical pumping power is 80 mW. The solid curves for $[g^{(2)}_{s,as}]_m$ are theoretical plots obtained by taking into account the uncorrelated noise photons.
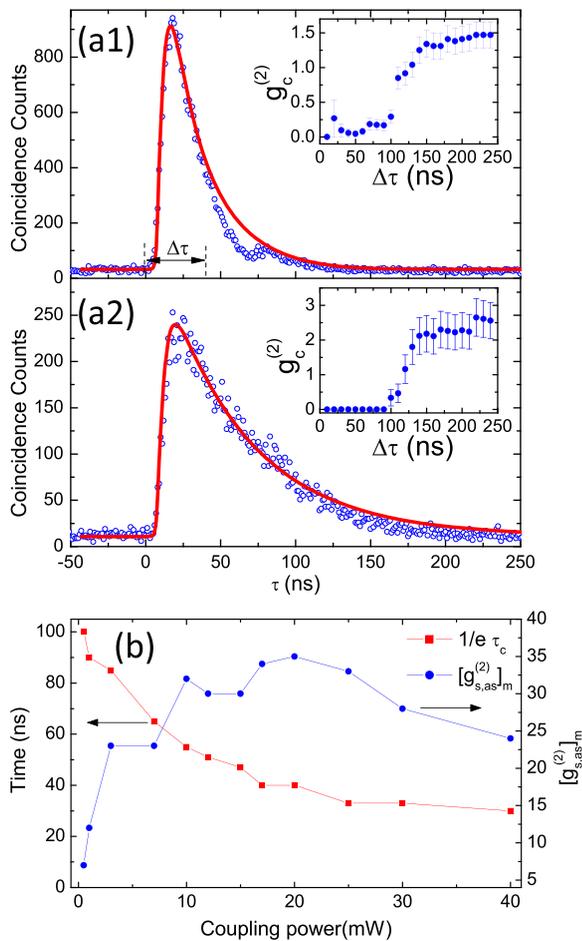
FIG. 5. Biphoton generation with controllable coherence time. (a) Two-photon coincidence counts collected over 300 s with 1 ns bin width as a function of the relative time delay τ with two different coupling laser powers: (a1) 20 mW and (a2) 3 mW. For the case of (a1) with 20 mW coupling power, the biphoton correlation time (bandwidths) is 40 ns (4.0 MHz). As we reduce the coupling power to 3 mW, the biphoton correlation time (bandwidths) increases (decreases) to 85 ns (1.9 MHz) as shown in (a2). The pump laser power is fixed at 6 mW. The insets show the corresponding measured conditional auto-correlation function $g_c^{(2)}$ of heralded anti-Stokes photons. The error bars in the data plots are the standard error which can be reduced with longer data taking time. (b) $1/e$ correlation time and $[g_{s,as}^{(2)}]_m$ as functions of the coupling laser power.

[1]H. J. Kimble, "The quantum internet," Nature **453**, 1023 (2008).

[2]C.-S. Chuu, G. Y. Yin, and S. E. Harris, "A miniature ultrabright source of temporally long, narrowband biphotons," Appl. Phys. Lett. **101**, 051108 (2012).

[3]M. Scholz, L. Koch, R. Ullmann, and O. Benson, "Single-mode operation of a high-brightness narrow-band single-photon source," Appl. Phys. Lett. **94**, 201105 (2009).

[4]J. Fekete, D. Rielander, M. Cristiani, and H. de Riedmatten, "Ultranarrow-band photon-pair source compatible with solid state quantum memories and telecommunication networks," Phys. Rev. Lett. **110**, 220502 (2013).

[5]S. Du, P. Kolchin, C. Belthangady, G. Y. Yin, and S. E. Harris, "Subnatural linewidth biphotons with controllable temporal length," Phys. Rev. Lett. **100**, 183603 (2008).

[6]L. Zhao, X. Guo, C. Liu, Y. Sun, M. M. T. Loy, and S. Du, "Photon pairs with coherence time exceeding one microsecond," Optica **1**, 84 (2014).

[7]L. Zhao, Y. Su, and S. Du, "Narrowband biphoton generation in the group delay regime," Phys. Rev. A **93**, 033815 (2016).

[8]C. Shu, P. Chen, T. K. A. Chow, L. Zhu, Y. Xiao, M. M. T. Loy, and S. Du, "Subnatural-linewidth biphotons from a Doppler-broadened hot atomic vapour cell," Nat. Commun. **7**, 12783 (2016).

[9]S. Du, J. Wen, and M. H. Rubin, "Narrowband biphoton generation near atomic resonance," J. Opt. Soc. Am. B **25**, C98 (2008).

[10]M. D. Reid and D. F. Walls, "Violations of classical inequalities in quantum optics," Phys. Rev. A **34**, 1260 (1986).

[11]D. A. Stek, see http://steck.us/alkalidata for Rubidium 87 D line data.

[12]P. Grangier, G. Roger, and A. Aspect, "Experimental evidence for a photon anticorrelation effect on a beam splitter: A new light on single-photon interferences," Europhys. Lett. **1**, 173 (1986).

[13]L.-M. Duan, M. D. Lukin, J. I. Cirac, and P. Zoller, "Long-distance quantum communication with atomic ensembles and linear optics," Nature **414**, 413 (2001).

[14]A. K. Ekert, "Quantum cryptography based on Bells theorem," Phys. Rev. Lett. **67**, 661 (1991).

[15]C. Liu, S. Zhang, L. Zhao, P. Chen, C.-H. Fung, H. F. Chau, M. M. T. Loy, and S. Du, "Differential-phase-shift quantum key distribution using heralded narrow-band single photons," Opt. Express **21**, 9505 (2013).